Cascades Field Analysis of Axial Flow Turbine Stage in Al-Hilla Gas Turbine Power Station by Using Fluent Technique

Arkan K. Al-taie *University of Baghdad*

Saba Y. Ahmed *University of Babylon*

Abstract

In the present research, flow through rotor-stator of first stage of axial flow turbine in Al-Hilla Gas Turbine Power Plant is analyzed. This 2D analysis provides insight into the accuracy of the discretization scheme and FLUENT's ability to predict the complicated flow features typical of turbo machinery applications. The analysis method is based on unsteady, two dimensional, compressible, inviscid flow with steady-state solutions computed as the asymptotic limit in time of transient solution. Two turbine blade cases are presented. The first involves subsonic flow throughout the rotor blade turbine; the second involves subsonic inlet and discharge flows with transonic flow over a portion of the blade passage. Generally good results is shown.

الخلاصة

في هذا البحث تم تحليل الجريان ثنائي الأبعاد خلال كلاً من الريشة المتحركة والثابتة للمرحلة الأولى للتوربين المحوري في محطة كهرباء الحلة الغازية ، وذلك باستخدام برنامج الـFLUENT وطريقة الشابك ألانزلاقي , حيث انماز البرنامج بالقدرة على تحليل كافة أساليب الجريان المعقدة وخاصةً في تطبيقات المحركات التوربينية . إن طريقة التحليل اعُتمدت على فرض الجريان ؛ غير مستقر ؛ ثنائي الأبعاد ؛ انضغاطي ؛ غير لزج ؛ مع الأخذ بنظر الاعتبار حالة الجريان المستقر كظروف ابتدائية لحالة الجريان الغير المستقر وفي هذا البحث أيضاً تم دراسة حالتين للجريان المار خلال الريشة المتحركة للتوربين ، الحالة الأولى: حالة الجريان دون الصوتي بالاعتماد على قيمة الضغط الخارج من الريشة المتحركة ؛ والحالة الثانية هي حَوْلَ الصوتي :دون الصوتي وفوقه وقد حققت كِلا الحالتين نتائج جيدة.

Nomenclature

C	Chord Line
M	Mach number
P	Static pressure
P_o	stagnation pressure
R	Radius
T	Passing period
U	Axial velocity
V	Radial velocity
Subscripts	
1	Uniform state upstream of rotor-stator blade
2	Uniform state downstream of rotor-stator blade
x	Axial direction
Abbreviation	
CFL	Courant-Friedrichs-Lewy
CFD	Computational Fluid Dynamic

1.Introduction

The flow through an axial turbo-machines is primarily in the axial direction. Axial flow turbo-machines have airfoil- shaped surfaces, called blades, attached to the periphery of a rotating disk spokes on a hub. The unit is known as a rotor and is usually enclosed by a casing to minimize leakage over the tips of the blades. The fluid flows axially through the annular space between the hub and casing, Figure (1) shows the principle of the axial flow rotor. Many axial flow machines have sets of alternating moving blades and stationary surfaces called vanes. The vanes are also airfoil- shaped and are attached to the inside of the casing. A circumferential set of vanes is called a stator. The stator does not change the mechanical energy of the flow but simply alters the proportion between static and dynamic pressure. Since the fluid is confined, substantial changes in static pressure can occur. One rotor and its adjacent down stream stator are called a stage. Some axial flow compressor may have as many as 15 stages, axial flow turbines usually have no more than three stages.

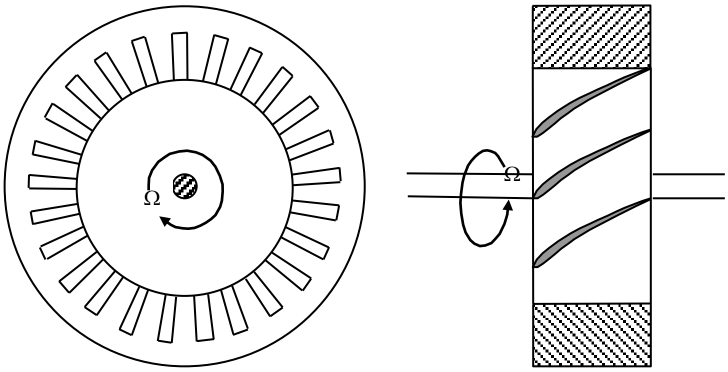

Figure(1): Axial Flow Rotor (Mironer, Alan, 1979).

The determination of the steady two dimensional isentropic flow field in the blade passages of an axial flow turbine is difficult, because the partial differential equation governing subsonic flow are elliptic. Consequently the solution at every point in the flow field depends on all of the boundary data simultaneously. In the case of an unsteady two dimensional isentropic flow of an inviscid fluid, however, the governing equations are hyperbolic, and the method of characteristics may be employed for determining the flow field. Delaney and Kavanagh, 1976 are developed a complete computer program based on pentahedral bi-characteristic curve network proposed by Butler, 1960. They apply a second order time dependent method characteristics using bi-characteristics. Their inverted scheme fixes the solution point in the new time plane determined by the time increment and the bi-characteristics and particle path are projected back from the solution point into the initial data plane. This permits the use of a regular finite difference grid formed by equally spaced quasi-orthogonal and quasi-streamlines. The streamline curvature method has been widely used in calculating through flow behavior, whilst several restriction were originally placed on both the grid and the positions of the calculation stations, modern versions of this technique have eliminated such restrictions, among workers in this method, we can cite Katsanis, 1968, Smith, 1966, Novak, 1967 and Frost, 1970. Finite element solutions of the through flow problem are presented by Hirsch and Warzee, 1976, Oates, Knight and Carey, 1976. An interesting discussion by Sapikes at the end of Hirsch and Warzee, 1976 article, provides the impetus for a streamline curvature/ finite element comparison. Currently, turbomachinery analysis consider two extreme. The overall machine is broadly designed using throughflow techniques(like streamline curvature)which rely heavily on a mature database(for loss and deviation for example). AGARD AR-175, 1989, describes this sort of approach in detail. The individual blade rows are examined using 2D or 3D Euler or Navier-Stokes solvers, nominally at an operating point similar to that supplied from the through flow analysis, but really run as if in an isolated cascade AGARD LS-140, 1985, VKI-LS-2, 1986, Dawes, 1990. Computational Fluid Dynamic (CFD) simulation has become an essential tool in the design and analysis of modern turbomachinery components during the past decade. Steady and unsteady state flow predictions are widely studied for problem ranging from a single turbine blade to a complete multistage turbomachine and MUSCL-type approach is used for achieving higher-order accuracy Guha, and Mei, 2005.

2. Purpose of This Research

In this research, we focus our attention on a specific axial flow turbo-machines, by considering a first stage of an axial flow turbine of Al-Hilla gas turbine power plant to analyze the flow between the stator–rotor blade by using fluent technique*, and the flow between vanes and blades will be considered as unsteady, compressible, inviscid, and turbulent flow.

3. Problem Description

3.1 Turbine Section

The turbine is where the high temperature gases from the combustion section are converted to shaft horsepower. The power required to drive the load package and compressor rotor is provided by the two stage turbine rotor. The first stage, or high pressure wheel and the second-stage, or low pressure wheel bolted together to make up a single unit through which the first and second stage nozzles direct the flow of combustion gases. These components, with associated air seals and deflectors are contained within the turbine shell. Figure (2) illustrate schematically the planar slice through the rotor and stator blades, extracted by unrolling a plane of constant radius (R=0.658 m). the speed of rotation , 5100 r.p.m, yields a linear velocity of the rotor, ΩR, equal to 351.48531 m/sec as indicated in Figure (2).

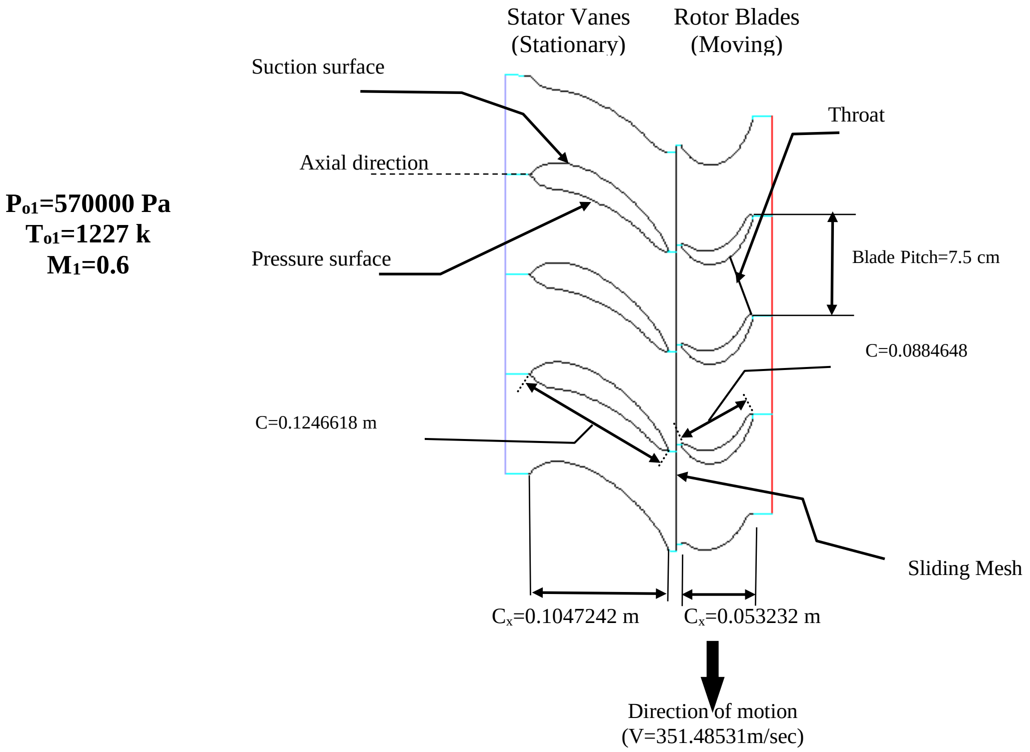

Stagger Angle Stator=28.5°; Stagger Angle for Rotor=27°
Airfoil camber Angle for Stator =60°; Airfoil camber Angle for Rotor=109°
Incidence Angle for Stator=0°

Figure (2): Rotor-Stator Problem Description.

3.2. Grid Generation and Boundary Conditions:

3.2.1 Grid Generation

*** Fluent is a state -of-the –art computer program for modeling fluid flow and heat transfer in complex geometric, fluent is written in the C computer language and makes full use of the flexibility and power offered by the language in addition fluent, provides complete mesh flexibility, solving your flow problems with unstructured meshes that can be generated about complex geometries with relative case. Supported mesh types includes 2D triangle / quadrilateral 3D tetrahedral /hexahedral/ pyramid / wedge, and mixed (hybrid) meshes. Fluent also allows you to refine or coarsen your grid based on the flow solution.**

The geometries of the stator and rotor flow domain have been meshed separately, this is usual procedure when the sliding mesh capability is used, for stator vane the finite difference mesh is (71*11) grid is used while for the rotor blade is (71*16) as shown in Figure (3).

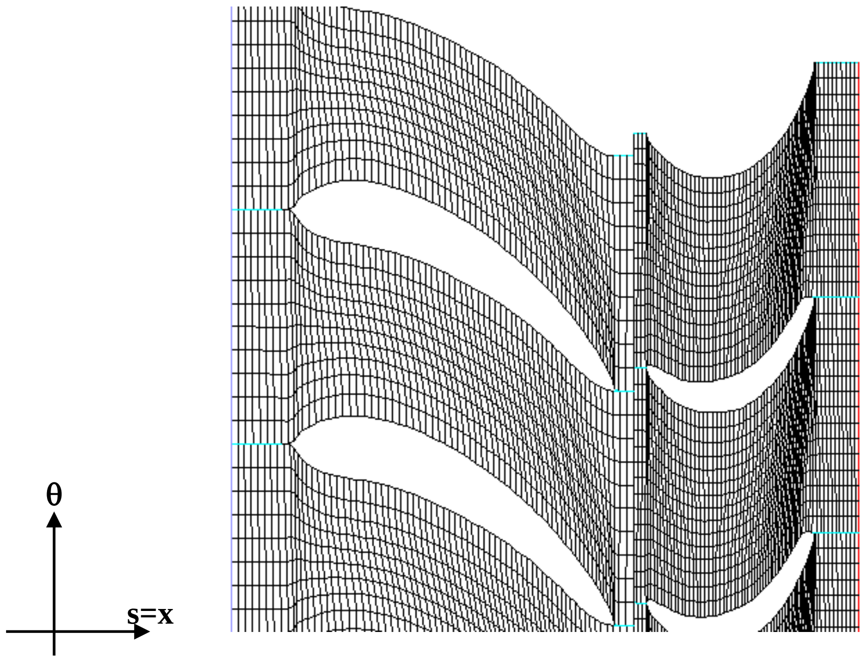

Figurer (3):Rotor-Stator Mesh Display.

The Sliding Mesh Technique:

In the sliding mesh technique two or more cell zones are used. Each cell zone is bounded by at least on " interface zone" where it meets the opposing cell zone. The interface zone of adjacent cell zones are associated with one another to form a " grid interface" the two cell zones will move relative to each other along the grid interface. Note that the grid interface must be positioned so that it has fluid cells on both sides, for example, the grid interface for the geometry shown in Figure(2) must lie in the fluid region between the rotor and stator ; it cannot be on the edge of any part of the rotor or stator. During the calculation, the cell zones slide (i.e., rotate or translate) relative to one another along the grid interface in discrete steps Jameson*, et. al.,* 1981.

Grid Interface Shapes

The grid interface and the associated interface zones can be any shapes, provided that the two interface boundaries are based on the same geometry. Figure (4) shows an example with a linear grid interface and Figure (5) shows a circular-arc grid interface. In both figures, the grid interface is designed by a dashed line Jameson, A., et. al., 1981. In this research we used the Figure(4).

.

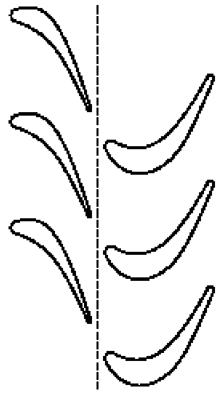

Figure(4): 2D Linear Grid Interface.

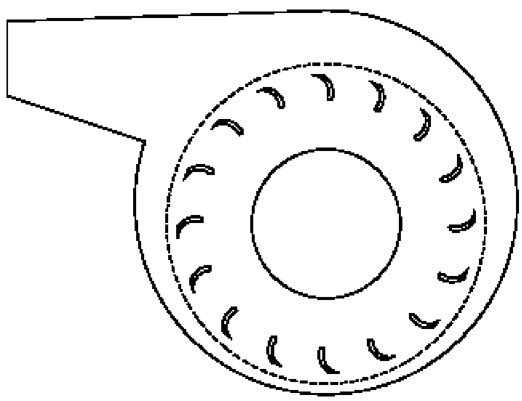

Figure (5): 2D Circular- Arc Grid Interface.

3.2.2 Governing Equations:

The governing equations for the model used in this research are the compressible, continuity, momentum equation, and energy equations written in an integral form where the volume of a computational cell is denoted by V

$$\frac{\partial}{\partial t}\int_V W\, dV + \oint \left| F - G \right| \cdot dA = \int_V H\, dV \qquad \ldots(1)$$

Where the vectors W, F, and G are defined as

$$W = \begin{pmatrix} \rho \\ \rho u \\ \rho v \\ \rho w \\ \rho E \end{pmatrix},\ F = \begin{pmatrix} \rho \\ \rho v u + pi \\ \rho v v + pj \\ \rho v w + pk \\ \rho v E + pv \end{pmatrix},\ G = \begin{pmatrix} 0 \\ \tau_{xi} \\ \tau_{yi} \\ \tau_{zi} \\ \tau_{ij} v_j + q \end{pmatrix}$$

And the vector H contains source term such as body forces and energy sources. Here ρ, υ, E, and p are the density, velocity, total energy per unit mass, and pressure of the fluid, respectively. τ is the viscous stress tensor, and q is the heat flux. Total energy E is related to the total enthalpy H by

$$E=H-p/\rho \qquad \ldots(2)$$

$$H = h + \left| v \right|^2 / 2 \qquad \ldots(3)$$

The Navier-Stokes equations as expressed in equation(1) become (numerically) very stiff at low Mach number due to the disparity between the fluid velocity υ and the acoustic speed c(speed of sound). This is also true for incompressible flows, regardless of the fluid velocity, because acoustic waves travel infinitely fast in an incompressible fluid (speed of sound is infinite). The numerical stiffness of the equations under these conditions results in poor convergence rates. This difficulty is overcome in Fluent's coupled solver by employing a technique called (time derivative) preconditioning Westbrook, and Dryer, 1981.

3.2.3 Preconditioning

Time derivative preconditioning modifies the time derivative term in equation (1) by pre-multiplying it with a preconditioning matrix. This has the effect of re-calling the acoustic speed (eigenvalues) of the system of equations being solved in order to alleviate the numerical stiffness encountered in low Mach number and incompressible. Derivation of the preconditioning matrix begins by transforming the dependent variable in equation (1) from conserved quantities W primitive variable Q using chain-rule as follows:

$$\frac{\partial W}{\partial Q}\frac{\partial}{\partial t}\int_V Q\,dV + \oint \left|F - G\right| \cdot dA = \int_V H dV \qquad \ldots(4)$$

Where Q is the vector $\left(\rho \quad u \quad v \quad w \quad T\right)^T$ and the Jacobian $\partial W/\partial Q$ is given by

$$\frac{\partial W}{\partial Q} = \begin{pmatrix} \rho_p & 0 & 0 & 0 & \rho_T \\ \rho_p u & \rho & 0 & 0 & \rho_T u \\ \rho_p v & 0 & \rho & 0 & \rho_T v \\ \rho_p w & 0 & 0 & \rho & \rho_T w \\ \rho_p H - \delta & \rho u & \rho v & \rho w & \rho_T H + \rho C_p \end{pmatrix} \qquad \ldots(5)$$

Where

$$\rho_p = \left.\frac{\partial \rho}{\partial p}\right|_T \quad , \ \rho_T = \left.\frac{\partial \rho}{\partial T}\right|_p$$

and δ=1 for an ideal gas and δ=0 for an incompressible fluid. The choice of primitive variables Q as dependent variables is desirable for several reasons. First it is a natural choice when solving incompressible flows. Second, when we use second order accuracy we need to reconstruct Q rather than W in order to obtain more accurate velocity and temperature gradients in viscous fluxes, and pressure gradients in invscid fluxes. And finally, the choice of pressure as a dependent variable allows the propagation waves in the system to be singled out Venkateswaran, *et al.*, 1992. The inviscid flux vector F appearing in equation (5) is evaluated by a standard upwind, flux difference splitting Roe, 1986. This approach acknowledge that the flux vector F contains characteristic information propagating through the domain with speed and direction according to the eigenvalues of he system. By splitting F into parts, where each part contains information traveling in a particular direction (i.e., characteristic information), and upwind differencing the split fluxes in a manner consistent with their corresponding eigenvalues, we obtain the following expression for the discrete flux at each face:

$$F = \frac{1}{2}\left(F_R + F_L\right) - \frac{1}{2}\Gamma\left|\hat{A}\right|\delta Q \qquad \ldots(6)$$

Here δQ is the special difference Q_R-Q_L. the fluxes $F_R=F(Q_R)$ and $F_L=F(Q_L)$ are computed using the (reconstructed) solution vectors Q_R and Q_L on the "right" and "left" side of the face. He matrix $|\hat{A}|$ is defined by

$$\left|\hat{A}\right| = M\left|\Lambda\right|M^{-1} \qquad \ldots(7)$$

Where Λ is the diagonal matrix of eigenvalues and M is the modal matrix that diagonalizes $\Gamma^{-1}|\hat{A}|$. Where A is the inviscid flux Jacobian $\partial F / \partial Q$.

3.2.4 Turbulence Model

3.2.4.1 The Standard k-ε Model

The standard k-ε model Launder, and Spalding, 1974 is a semi-empirical model based on model transport equations for the turbulent kinetic energy (k) and its dissipation rate (ε). The model transport equation for k is derived from the exact equation, while the model transport equation for ε was obtained using physical reasoning and bears little resemblance to its mathematically exact counterpart. In the derivation of the k-ε model, it was assumed that the flow is fully turbulent, and the effects of molecular viscosity are negligible. The standard k-ε model is therefore valid only for fully turbulent flows.

3.2.4.2 Transport Equations for the Standard k-ε Model

The turbulent kinetic energy, k, and its rate of dissipation, ε, are obtained from the following transport equations:

$$\rho\frac{Dk}{Dt} = \frac{\partial}{\partial x_i}\left[\left(\mu + \frac{\mu_t}{\sigma_k}\right)\frac{\partial k}{\partial x_i}\right] + G_k + G_b - \rho\varepsilon - Y_M \qquad \ldots(8)$$

And

$$\rho\frac{D\varepsilon}{Dt} = \frac{\partial}{\partial x_i}\left[\left(\mu + \frac{\mu_t}{\sigma_\varepsilon}\right)\frac{\partial \varepsilon}{\partial x_i}\right] + C_{1\varepsilon}\frac{\varepsilon}{k}\left(G_k + C_{3\varepsilon}G_b\right) - C_{2\varepsilon}\rho\frac{\varepsilon^2}{k} \qquad \ldots(9)$$

In these equations, G_k represents the generation of turbulent kinetic energy due to the mean velocity gradients, and calculated from

$$G_k = -\rho\overline{u_i'u_j'}\frac{\partial u_j}{\partial x_i} \qquad \ldots(10)$$

To evaluate G_k in a manner consistent with the Boussinesq hypothesis,

$$G_k = \mu_t S^2 \qquad \ldots(11)$$

Where S is the modulus of the mean rate of strain tensor, defined as

$$S \equiv \sqrt{2S_{ij}S_{ij}} \qquad \ldots(12)$$

With the mean strain rate S_{ij} given by

$$S_{ij} = \frac{1}{2}\left(\frac{\partial u_i}{\partial x_j} + \frac{\partial u_j}{\partial x_i}\right) \qquad \ldots(13)$$

G_b is the generation of turbulent kinetic energy due to buoyancy which is neglected here, and Y_M represents the contribution of fluctuating dilatation in compressible turbulence to the overall dissipation rate, this term is modeled according to a proposal by Sarkar and Balakrishnan, 1990

$$Y_M = \rho\varepsilon 2M_t^2 \qquad \ldots(14)$$

Where M_t is the turbulent Mach number, defined as

$$M_t = \sqrt{\frac{k}{a^2}} \qquad \ldots(15)$$

Where a($\equiv \sqrt{\gamma RT}$) is the speed of sound.

This compressibility modification always takes effect when the compressible form of the ideal gas law is used.

3.2.4.3 Modeling the Turbulent Viscosity

The "eddy" or turbulent viscosity, μ_t, is computed by combining k and ε as follows:

$$\mu_t = \rho C_\mu \frac{k^2}{\varepsilon} \qquad \ldots(16)$$

Where C_μ is a constant and the model constants $C_{1\varepsilon}$, $C_{2\varepsilon}$, $C_{3\varepsilon}$, σ_k and σ_ε have the following default values Launder, B. E. and Spalding, D. B., 1974

$C_{1\varepsilon}$ =1.44, $C_{2\varepsilon}$ =1.92, $C_{3\varepsilon}$ =0.09, σ_k =1.0, σ_ε=1.3.

3.2.4.4 Time Marching for Steady-State Flows

The coupled set of governing equation (4) in FLUENT is discretized in time for both steady and unsteady calculations. In the steady case, it is assumed that time marching proceeds until a steady state solution is reached. Temporal discretization of the coupled equations is accomplished by either an implicit or an explicit time-marching scheme. The implicit time- marching are used in this research .

Implicit Scheme

In the implicit scheme, an Euler implicit discretization in time of the governing equations (4) is combined with a Newton-type linearization of the fluxes to produce the following linearized system in delta form Weiss *et. al.*, 1997:

$$\left[D + \sum_{j}^{N_{faces}} S_{j,k} \right] \Delta Q^{n+1} = -R^n \qquad \ldots(17)$$

The center and off-diagonal coefficient matrices, D and $S_{j,k}$ are given by:

$$D = \frac{V}{\Delta t} \Gamma + \sum_{j}^{N_{faces}} S_{j,i} \qquad \ldots(18)$$

$$S_{j,k} = \left(\frac{\partial F_j}{\partial Q_k} + \frac{\partial G_j}{\partial Q_k} \right) \qquad \ldots(19)$$

and the residual vector R^n and time step Δt are defined as, respectively

$$R^i = \sum^{N_{faces}} F(Q^i) - G(Q^i).A - V\,H$$

$$\Delta t = \frac{CFL\ \Delta x}{\lambda_{max}}$$

where λ_{max} is the maximum of the local eigenvalues.

Equation (17) is solved using a point Gauss-Seidel scheme in conjunction with an algebraic multigrid (AMG) method adapted for coupled sets of equations.

Temporal Discretization for Unsteady Flows

For time-accurate calculations, explicit and implicit time-stepping schemes are available. (The implicit approach is also referred to as "dual time stepping".)

To provide for efficient, time-accurate solution of the preconditioned equations, we employ a dual time-stepping, multi-stage scheme. Here we introduce a preconditioned pseudo-time-derivative term into Equation (1) as follows:

$$\frac{\partial}{\partial t} \int_V W\, dV + \Gamma \frac{\partial}{\partial \tau} \int_V Q\, dV + \oint \left| F - G \right| \cdot dA = \int_V H\, dV \qquad \ldots(20)$$

where t denotes physical-time and τ is a pseudo-time used in the time marching procedure. Note that as $\tau \to \infty$, the second term on the LHS of Equation (20) vanishes and Equation (1) is recovered.

The time-dependent term in Equation (20) is discretized in an implicit fashion by means of either a first- or second-order accurate, backward difference in time. This is written in semi-discrete form as follows:

$$\left[\frac{\Gamma}{\Delta\tau}+\frac{\in_o}{\Delta t}\frac{\partial W}{\partial Q}\right]\Delta Q^{k+1}+\frac{1}{V}\oint\left[F-G\right].dA = H+\frac{1}{\Delta t}\left(\in_o W^{k}-\in_1 W^{n}+\in_2 W^{n-1}\right)$$
...(21)

where $\in_0 = \in_1 = 1=2$; $\in_2 = 0$ gives first-order time accuracy, and $\in_0 =3/2$; $\in_1 = 2$; $\in_2 = 1/2$ gives second-order. k is the inner iteration counter and n represents any given physical-time level. The pseudo-time-derivative is driven to zero at each physical time level by a series of inner iterations using either the implicit or explicit time marching algorithm. Throughout the (inner) iterations in pseudo-time, W^n and W^{n-1} are held constant and W^k is computed from Q^k. As $\tau \to \infty$, the solution at the next physical time level W^{n+1} is given by $W(Q^k)$. Note that the physical time step Δt is limited only by the level of desired temporal accuracy. The pseudo-time-step $\Delta\tau$ is determined by the CFL condition of the time-marching scheme Jameson, *et. al.*, 1981..

3.2.5 Boundary Conditions:

Boundary conditions for the network are: the upstream boundary points for stator vane, the downstream points for the rotor. The inlet and exit boundary panels are positioned sufficiently far from the vane and blade so that uniform flow property distributions may be assumed along them. At the upstream boundary points, the steady state stagnation pressure and temperature are specified(as exit from combustion chamber), and the whirl component of the velocity (i.e, the y-component of velocity at the entrance to the cascade) is specified as zero. At the downstream boundary points the steady state static pressure is specified **. The specific heat ratio of the combustion gases is assumed to be(γ=1.3) as shown in Figure (6).

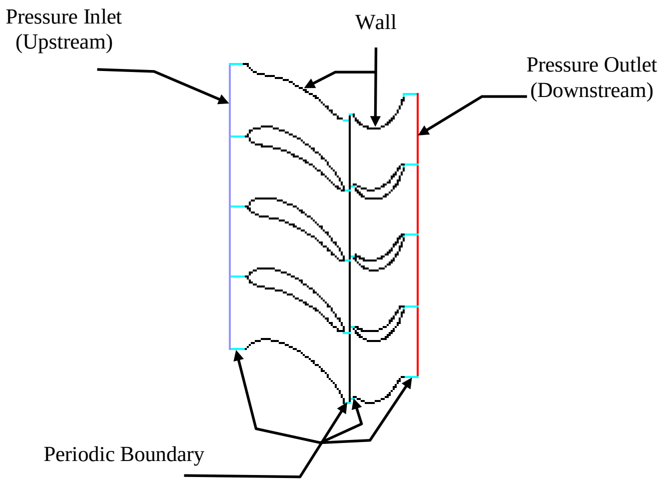

Figure(6): Boundary Condition for The Network.

** **Delaney(1) presented two cases of steady flow through a turbine cascade : one for subsonic flow throughout and one with region of transonic flow. The only difference between the subsonic and transonic flow cases is the value of the static pressure along the downstream boundary , denoted by p_2, for the subsonic flow case p_2=0.685 p_{o1}, while for the transonic flow case , p_2=0.578 p_{o1}, where p_{o1} is the steady state stagnation pressure along the upstream boundary. In both cases the whirl velocity component along the upstream boundary is zero, so that the velocity along the upstream boundary is in the axial direction.**

4. Coupled Solution Method

The coupled solver is the solution algorithm previously used by Fluent. This approach, using the governing equations of continuity, momentum, and energy equation are solved simultaneously (i.e., coupled together) as in equation (5). Governing equations for additional scalars will be solved sequentially (i.e., segregated from one another and from the coupled set) Because the governing equations are non-linear (and coupled), several iterations of the solution loop must be performed before a converged solution is obtained. Each iteration consists of the steps illustrated in Figure (7) and outlined below:

1. Fluid properties are updated, based on the current solution. (If the calculation has just begun, the fluid properties will be updated based on the initialized solution.)
2. The continuity, momentum, and energy equations are solved simultaneously .
3. Equations for scalars such as turbulence are solved using the previously updated values of the other variables.
4. A check for convergence of the equation set is made which is equal to 0.00001.

These steps are continued until the convergence criteria are met.

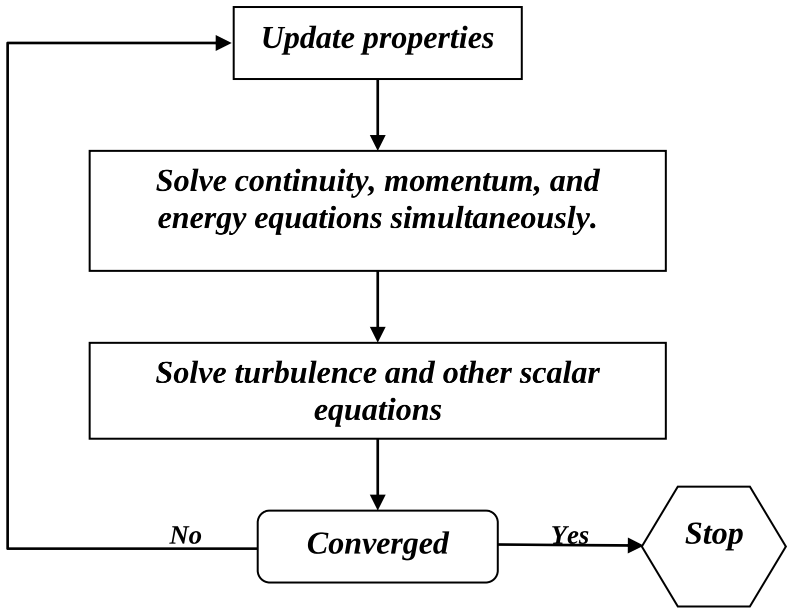

Figure (7): Overview of the Coupled Solution Method.

5.Results and Discussions:

Results computed for the two cases of unsteady flow through a blade passages of Al-Hilla Gas Turbine Power Plant are presented. The first case involves subsonic flow throughout the rotor-stator, and the second involves subsonic inlet and discharge flows, but with transonic flow over a portion of the blade passages. In both cases, the computed blade pressure and Mach number distribution are obtained.

For convenience, the results for the two example case are initially solved for steady flow through the blade passages. Later, the steady flow through the non-moving rotor passage will be present the starting point for the transient calculation. The selection of the time step is critical for accurate time dependent flow predictions. Here, the time step is chosen to be about 1/22 of the passing period, T***. The passing period is the time it takes for the rotor blade to pass from one stator blade row to the next:

$$T=(0.075m)/(351.45831m/s)= 2.1338018e-04$$

Using a time step of 0.00001second, 20 time steps will be performed as the rotor performs one pass.

The rotor-stator flow prediction will be continued in time until a time-periodic flow is obtained. Low accuracy during the initial passing periods is acceptable as long as convergence is achieved during each time step of the final passing periods.

Subsonic flow case: in this example, in addition to contain uniform inlet stagnation conditions, steady-state boundary conditions were prescribed as 1- zero whirl component along the upstream boundary for the stator, and 2-uniform normalized static pressure p_2=0685P_{o1}along the downstream boundary for the rotor, after 600 iterations, the steady flow calculation be fully converged as shown in Figure (8). Here, this is not of concern, as the steady-state prediction will be used only as a starting solution for the transient sliding-mesh calculation.

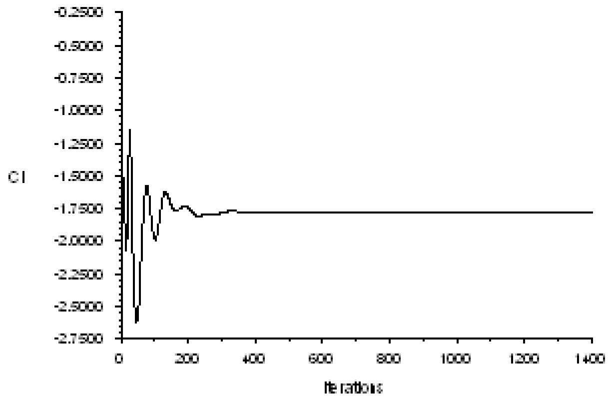

*** for some problems (e.g., rotor-stator interactions), you may be interested in a time-periodic solution. That is, the startup transient behavior may not be of interest to you. Once this startup has passed, the flow will star to exhibit time-periodic behavior. If T is the period of unsteadiness, then for some flow property $\phi(t)=\phi(t+NT)$ (N=1,2,3,….)

For rotating problems, the period (in seconds) can be calculated by dividing the sector angle of the domain (in radians) by the rotor speed (in radian/sec); $T=\theta/\Omega$. For 2D rotor-stator problems, $T=P/V_b$ where P is the pitch and V_b is the blade speed the number of time steps in a period can be determined by dividing the time period by the time step size. When the solution field does not change from one period to the next (for example, if the change is less than 5%), a time-periodic solution has been reached as mentioned in Fluent Inc user's guide, 1998, Meinhard, T. Schobeiri ,Burak, Öztürk, and David, E. Ashpis, 2003.

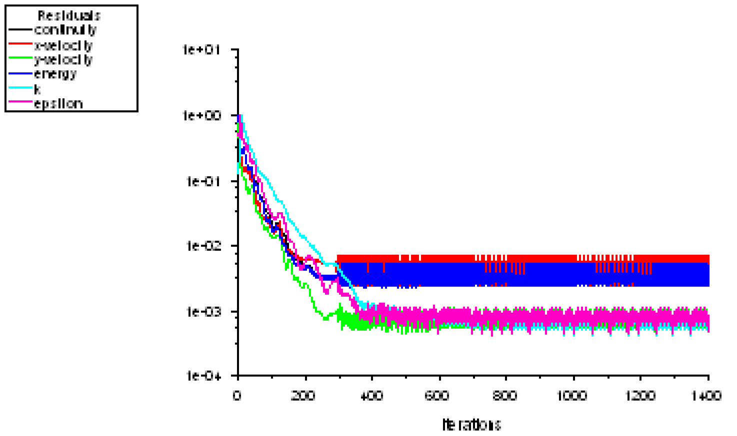

Figure (8): Lift Coefficient and Normalized Scaled Residual History; Steady Flow, Non-moving Rotor; Subsonic Flow Case; p_2=0.685P_{o1}.

By requesting 1019 time step this will include roughly 48 passing periods (48*T_{sec}=0.01019 sec). Figure(9) for the lift force coefficient history shows that the flow becomes time periodic approximately 0.0008(after about 4 passing periods).

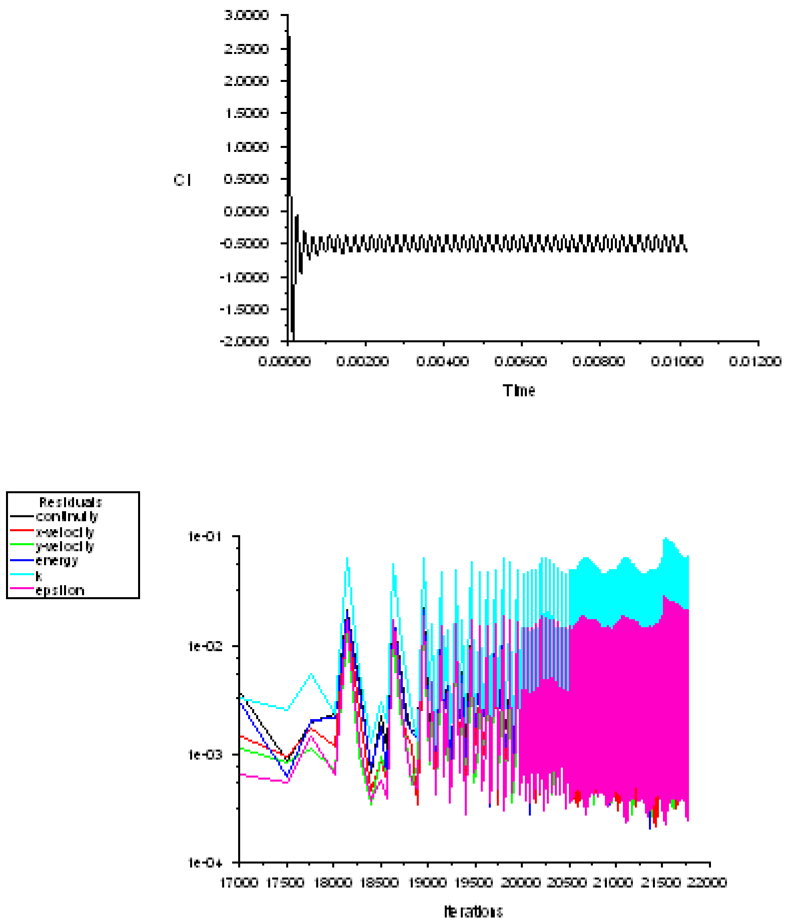

Figure (9): Lift Coefficient and Normalized Scaled Residual History; Unsteady Flow; moving Rotor; Subsonic Flow Case; p_2=0.685P_{o1}.

In Figure (10), the computed values of the blade surface static pressure for rotor are plotted versus axial distance x along the blade the lowest value of pressure occurs on the blade suction surface near the throat location for the blade passage

(x/C_x=0.6916) where C_x, is the blade axial chord. The pressure distribution on the rotor blade pressure surface indicate approximately uniform flow for x/C_x<0.6916, followed by accelerated flow to the trailing edge. On the blade suction surface the reverse is true, that is accelerated flow is indicated upstream of the throat, with nearly uniform flow downstream of the throat.

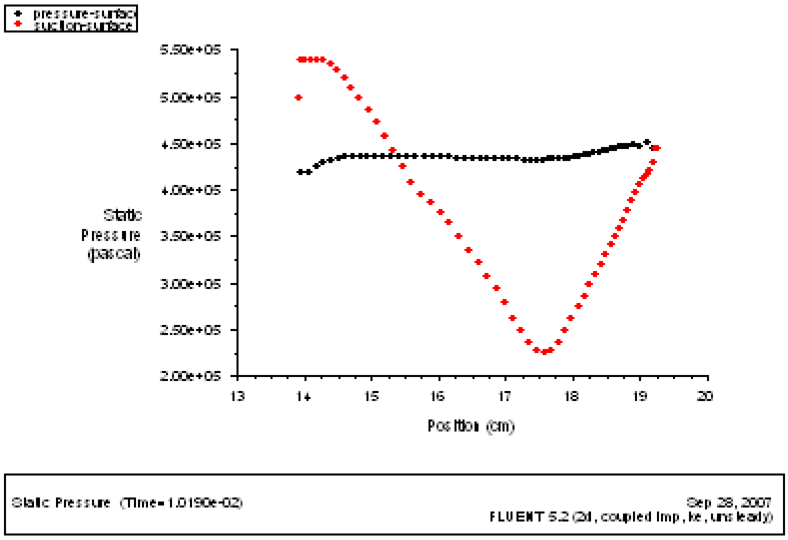

Figure (10): Rotor- Blade Surface Distribution of Static Pressure-Subsonic Flow Case; p_2=0.685P_{o1}.

Velocity vectors at every other point in the solution grid are shown in Figure(11) large velocity gradients are observed upstream of the passage throat for rotor, while downstream of the throat are approximately uniform distribution of the velocity can be seen. The velocity distribution around the leading edge of the rotor blade indicate that the stagnation point is located on the pressure surface of the blade. In the region of he upstream boundary, the velocity gradient in the axial direction is approximately zero. This tends to support the assumption of uniform whirl velocity distribution along the upstream boundary for stator.

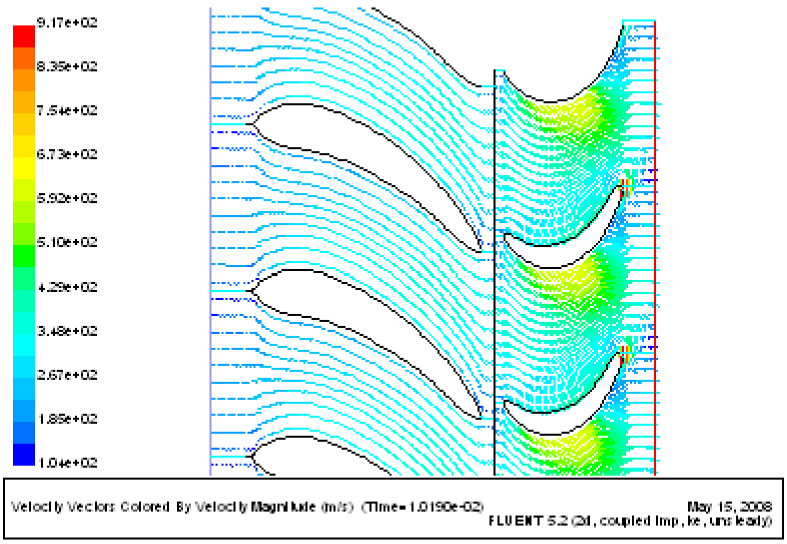

Figure (11): Velocity Vector Field; Subsonic Flow Case; p_2=0.685P_{o1}.

A contour plot of computed static pressure over the flow field is presented in Figure(12). The highly two-dimensional character of the flow is indicated. The maximum pressure gradient occur near the passage throat for rotor, with the minimum pressure occurring on the blade suction surface near the throat location. Upstream of the stator blade a nearly uniform pressure distribution is shown. At the downstream boundary, the axial pressure gradient are approximately zero, in support of the assumption of uniform static pressure along the downstream boundary.

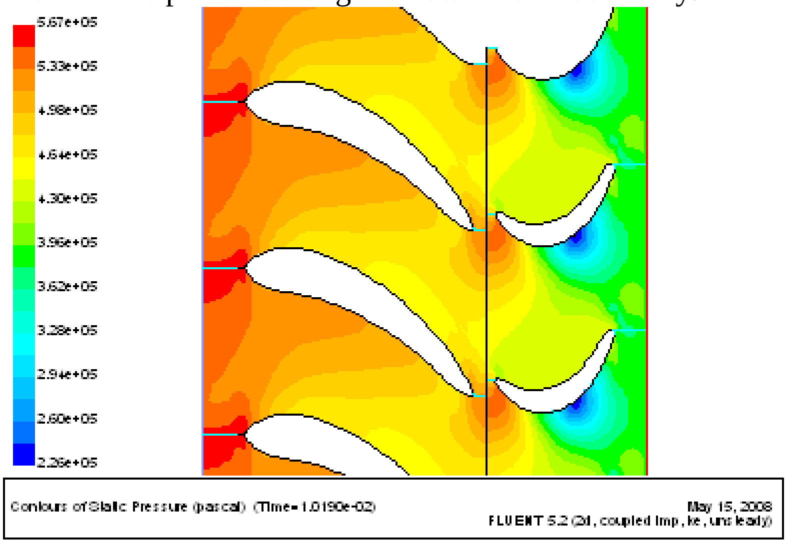

Figure (12): Contour of Static Pressure; Subsonic Flow Case; p_2=0.685P_{o1}.

Lines of constant Mach number in the flow field are shown in Figure(13). The contours indicate rapidly accelerating flow around the rotor blade leading edge on the suction surface and relatively uniform flow on the pressure surface near the leading edge.

Also, an approximately uniform distribution of Mach number is shown downstream of the throat on the blade suction surface. At the upstream boundary for stator, the contour lines are nearly horizontal indicating essentially zero Mach number gradient in the axial direction near the boundary.

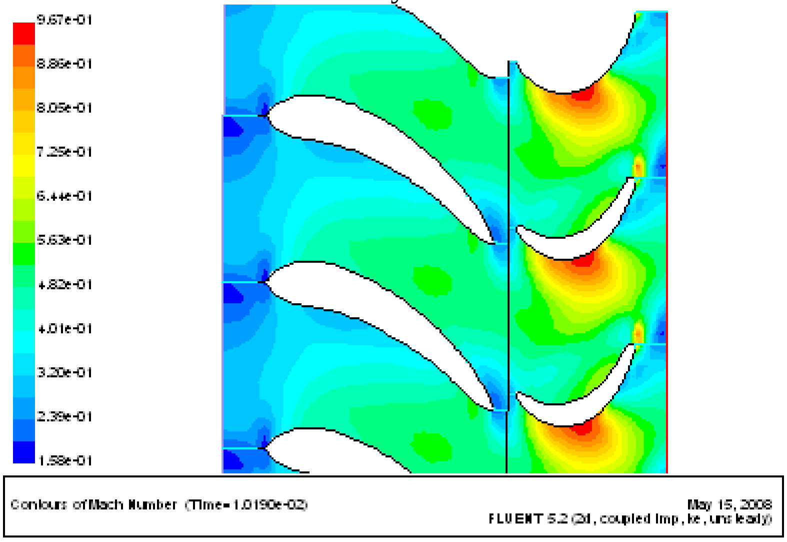

Figure (13): Contour of Mach Number; Subsonic Flow Case; p_2=0.685P_{o1}.

Transonic flow Case: the boundary conditions for this case flow example were the same as in the subsonic flow case except that the downstream normalized pressure $p_2=0.578P_{o1}$along the downstream boundary for the rotor. In this case, the flow accelerating to the transonic regime in the rotor blade passage. The initial data for the transient solution were taken from the steady state solution as mentioned in the subsonic flow, after 414 iterations, the steady flow calculation be fully converged as shown in Figure (14). Approximately 1041 time steps were required to obtain the steady flow results as presented in Figure (15).

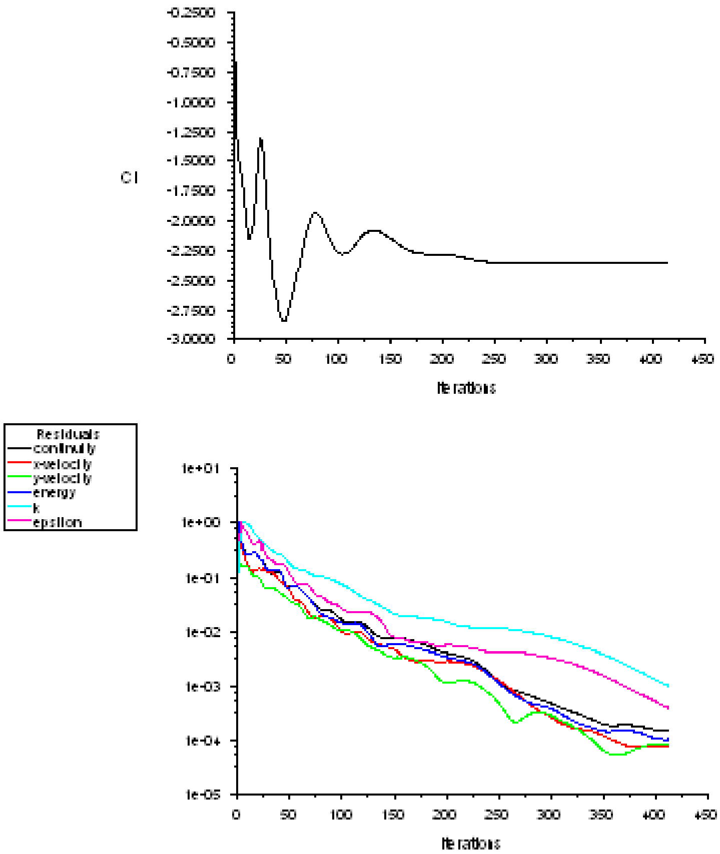

Figure (14): Lift Coefficient and Normalized Scaled Residual History; Steady Flow, Non-moving Rotor; Transonic Flow Case; $p_2=0.578P_{o1}$.

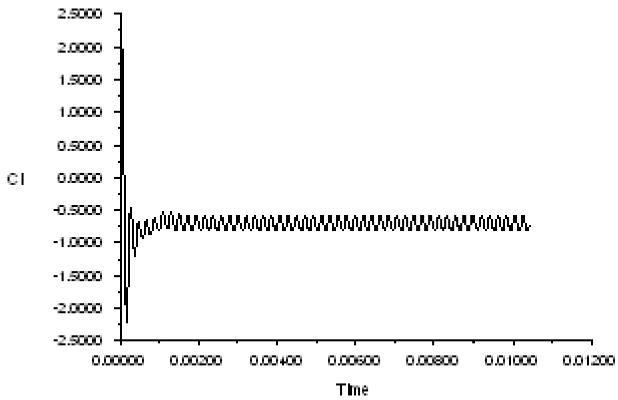

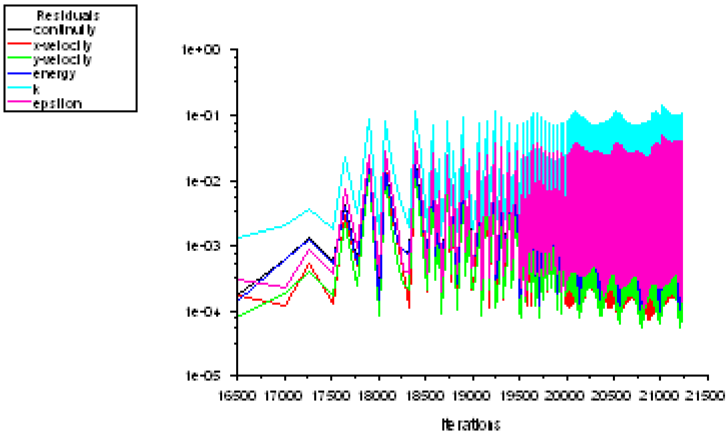

Figure (15): Lift Coefficient and Normalized Scaled Residual History; Unsteady Flow, moving Rotor; Transonic Flow Case; p_2=0.578P_{o1}.

In Figure(16), the pressure level on the blade suction surface of rotor indicates supersonic flow downstream of the throat. Also, the minimum blade surface pressure dose no occur at the blade throat as in the subsonic flow case, but further downstream at about (x/C_x=0.7573). The shifting of the minimum pressure point downstream of the throat is indicative of the fact that supersonic flow has been established. Comparison of blade pressure distribution in Fig.(16) and Fig.(10) for the two flow cases substantially higher blade loading in the transonic case with the majority of the loading increase occurring on the rear half of the rotor blade.

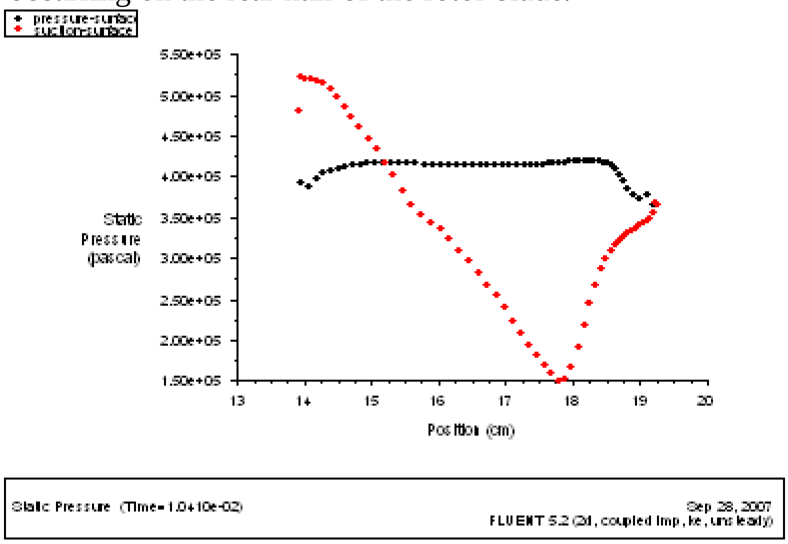

Figure (16): Rotor- Blade Surface Distribution of Static Pressure-Transonic Flow Case; p_2=0.578P_{o1}.

The velocity vector field for this example is presented in Figure(17). The influence of the blades on the upstream velocity distribution is again evident. Also, the leading edge stagnation point appears to be located in approximately the same location as in the subsonic flow case. However, one difference noted from the subsonic case is the increased velocity level which exists downstream of the throat.

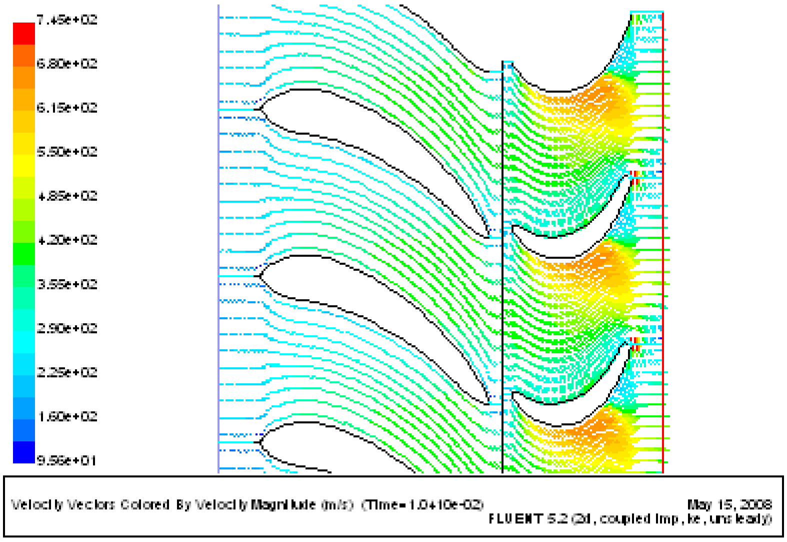

Figure (17): Velocity Vector Field; Transonic Flow Case; p_2=0.578P_{o1}.

A contour plot of static pressure is presented in Figure(18) . as in the subsonic flow case, a nearly uniform distribution of static pressure exists upstream of the rotor blade. The contour line distribution of static pressure for the subsonic and transonic flow cases in Figures(12),(18), respectively, are nearly the same upstream of the passage throat, indicating that both flow cases are close to the chocked condition. Much higher pressure gradients are shown downstream of the passage throat for the transonic flow case in Figure (18). Also, as has been noted already, it is apparent in Figure(18) that the minimum pressure point location has moved downstream to a point near rotor blade trailing edge on the suction surface.

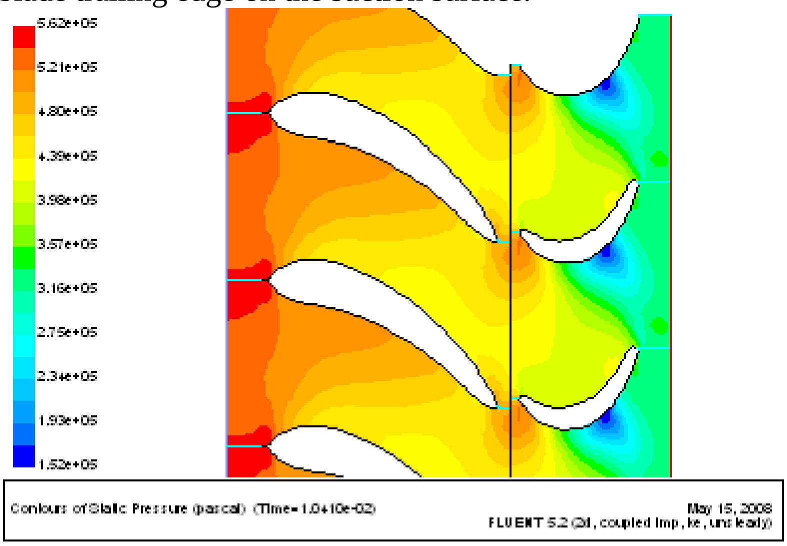

Figure (18): Contour of Static Pressure; Transonic Flow Case; p_2=0.578P_{o1}.

Lines of constant Mach number in the flow field are shown in Figure(19). The supersonic flow region is located on the rotor blade suction surface near the trailing edge. Again, the contour line distribution upstream of the throat is nearly the same as that in Figure(13) for the subsonic flow case.

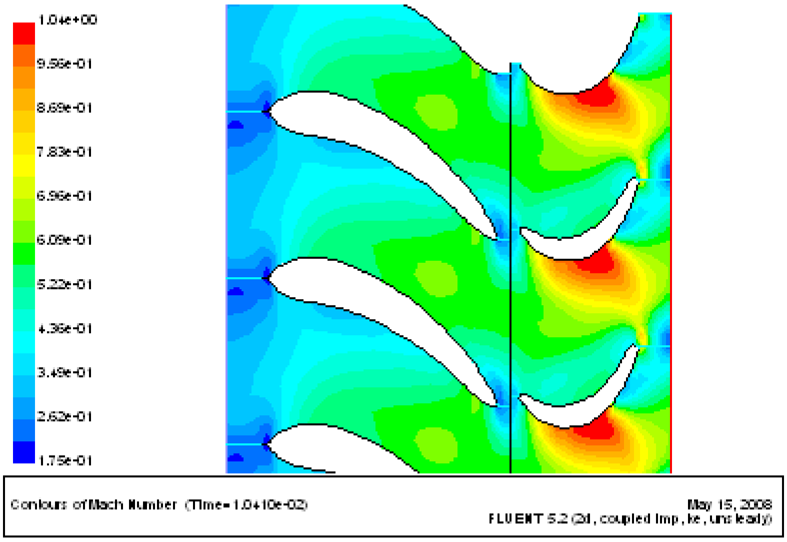

Figure (19): Contour of Mach Number; Transonic Flow Case; p_2=0.578P_{o1}.

6-Conclusions:

In this research we have modeled the time periodic flow involving rotor-stator interaction in Al-Hilla Gas Turbine Power Station and we have learned how to create the grid interface zones along the sliding mesh by using FLUENT technique. Steady state flows are computed as the asymptotic limit of transient solutions. Two turbine blade flow examples have been presented. One example involves subsonic flow throughout the rotor blade of turbine, while the other involves transonic flow over a region of the rotor blade passage. The success of the present model in solution of blade to blade flows in turbine stage suggests that the method could be extended for solution of hub-to-tip flow on an arbitrary stream surfaces in rotating blade rows.

7-Refernces

AGARD AR-175, (1981) "Through flow Calculations in Axial Turbomachines" Propulsion and Engineering Panel Working Group 12.

AGARD LS-140, (1985). "3D Computation Technique Applied to Internal Flows in Propulsion System" AGARD Lecturer Series No. 140.

Butler, D.S., (1960). "The Numerical Solution of Hyperbolic System of Partial Differential Equations in Three Independent Variables", Proceedings of Royal Society of London, Vol.255A, pp.232-252

Dawes, W.N., (1990). "Towards Improved Throughflow Capability: the Use of 3D Viscous Flow Solvers in a Multistage Environment", Trans. ASME J. of Turbomachinery presented as 90-GT-18.

Delaney, R.A., Kavanagh, P., (1976) "Transonic Flow Analysis in Axial Flow Turbomachinary Cascade by a Time Dependent Method Characteristic", Transactions of the ASME, July, pp.356-364, 1976.

Fluent User's Guide, vol.1,2,3, and 4, 1998

Frost, D.H., (1970) "A Stream Line Curvature Through Flow Computer Program for Analyzing the Flow Through Axial Flow Turbomachines", N.G.T,E., report No.312,1970.

Guha, A., and Mei, Y.; (2005) "Implicit Numerical Simulation of Transonic Flow through Turbine Cascades on unstructured grids",Proc.IMechE, Vol.219, Part A: J. Power and Energy, 2005.

Hirsch, C.H. and Warzee, G., (1976) "A Finite Element Method for Through Flow Calculation in Trubomachines", Journal of Fluid Engineering, Trans. ASME, pp.403-421, 1976.

Hirsch, C.H. and Warzee, G., (1976). "A Finite Element Method for the Axisymmetric Flow Computation in Turbomachine", Inst. for Numerical Methods in Engineering, pp.93-113.

Jameson, A., Schmidt, W., and Turkel, E. ,(1981). "Numerical Solution of the Euler Equations by Finite Volume Methods Using Runge-Kutta Time-Stepping Schemes". Technical Report AIAA-81-1259, AIAA 14th Fluid and Plasma Dynamics Conference, Palo Alto, Califorina, June.

Katsani, T., (1968). "A Computer Program for Calculating Velocities and Streamline on Blade to Blade Stream Surface of a Turbomachine", NASA-TN-D-4525.

Launder, B.E. and Spalding, D.B.; (1974). "The Numerical Computation of Turbulent Flows"; Computer Methods in Applied Mechanics and Engineering, 3:269-289.

Meinhard, T. Schobeiri , Burak Öztürk, David, E. Ashpis (2003). "On the Physics of Flow Separation Along a Low Pressure Turbine Blade Under Unsteady Flow Conditions"; NASA/TM-212290.

Mironer, Alan (1979). "Engineering Fluid Mechanic", McGraw-Hill, Inc..

Novak, R.A., (1967). "Streamline Curvature Computing Procedures for Fluid Flow Problems"; Journal of Engineering for Power, Trans. ASME, pp.478-490.

Oates, G.C., Knight, C.J. and Cary, G.F.,(1976). "A Variational Formulation of the Compressible Through Flow Problem", Journal of Engineering for Power, pp.1-8.

Roe, P.L., (1986). "Characteristic based schemes for the Euler equations"; Annual Review of Fluid Mechanics, 18:337-365.

Sarkar, S. and Balakrishnan, L.; (1990). "Application of a Reynolds-Stress Turbulence Model to the Compressible Shear Layer"; ICASE Report 90-18, NASA CR 182002.

Smith, L.H., (1966). "The Radial-Equilibrium Equation of Turbomachinary"; Journal of Engineering for Power, Trans. ASME, pp.1-12.

Venkateswaran, S., Weiss, J.M., and Merkle, C.L., (1992). "Propulsion Related Flow fields Using the Preconditioned Navier-Stokes Equations", Technical Report AIAA-92-3437, AIAA/ASME/SAE/ASEE 28th Joint Propulsion Conference, Nashville, TN, July.

VKI LS-2, (1986). "Numerical Technique for Viscous Flow Calculations in Turbomachinery Blading" Von Karman Institute Lecture Series Number 2.

Weiss, J. ; Maruszewski , M.,J.P., and Smith, W. A., (1997). "Implicit Solution of the Navier-Stokes Equations on Unstructured Meshes", Technical Report AIAA-97-2103, 13th AIAA CFD Conference, Snowmass, CO, July

Westbrook, C. and Dryer, F., (1981). "Simplified Reaction Mechanisms for Oxidation of Hydrocarbon Fuels in Flames". Comb. Sci. Tech, 27:31-43.